Dietary options and behavior suggested by plant biomarker evidence in an early human habitat

Clayton R. Magill[a,1], Gail M. Ashley[b], Manuel Domínguez-Rodrigo[c], and Katherine H. Freeman[d]

[a]Geological Institute, ETH Zürich, Zurich 8092, Switzerland; [b]Department of Earth and Planetary Sciences, Rutgers University, Piscataway, NJ 08854; [c]Department of Prehistory, Complutense University, Madrid 28040, Spain; and [d]Department of Geosciences, The Pennsylvania State University, University Park, PA 16802

Edited by Thure E. Cerling, University of Utah, Salt Lake City, UT, and approved January 21, 2016 (received for review April 13, 2015)

The availability of plants and freshwater shapes the diets and social behavior of chimpanzees, our closest living relative. However, limited evidence about the spatial relationships shared between ancestral human (hominin) remains, edible resources, refuge, and freshwater leaves the influence of local resources on our species' evolution open to debate. Exceptionally well-preserved organic geochemical fossils—biomarkers—preserved in a soil horizon resolve different plant communities at meter scales across a contiguous 25,000 m^2 archaeological land surface at Olduvai Gorge from about 2 Ma. Biomarkers reveal hominins had access to aquatic plants and protective woods in a patchwork landscape, which included a spring-fed wetland near a woodland that both were surrounded by open grassland. Numerous cut-marked animal bones are located within the wooded area, and within meters of wetland vegetation delineated by biomarkers for ferns and sedges. Taken together, plant biomarkers, clustered bone debris, and hominin remains define a clear spatial pattern that places animal butchery amid the refuge of an isolated forest patch and near freshwater with diverse edible resources.

biomarker | leaf wax | carbon isotope | paleoecology | human evolution

Spatial patterns in archaeological remains provide a glimpse into the lives of our ancestors (1–5). Although many early hominin environments are interpreted as grassy or open woodlands (6–8), fossil bones and plant remains are rarely preserved together in the same settings. As a result, associated landscape reconstructions commonly lack coexisting fossil evidence for hominins and local-scale habitat (microhabitat) that defined the distribution of plant foods, refuge, and water (7). This problem is exacerbated by the discontinuous nature and low time resolution often available across ancient soil (paleosol) horizons, including hominin archaeological localities. One notable exception is well-time-correlated 1.8-million-y-old paleosol horizons exposed at Olduvai Gorge. Associated horizons contain exceptionally preserved plant biomarkers along with many artifacts and fossilized bones. Plant biomarkers, which previously revealed temporal patterns in vegetation and water (8), are well preserved in the paleosol horizon and document plant-type spatial distributions that provide an ecosystem context (9, 10) for resources that likely affected the diets and behavior of hominin inhabitants.

Plant biomarkers are delivered by litter to soils and can distinguish plant functional type differences in standing biomass over scales of 1–1,000 m^2 (11). Trees, grasses, and other terrestrial plants produce leaf waxes that include long-chain *n*-alkanes such as hentriacontane (nC_{31}), whereas aquatic plants and phytoplankton produce midchain homologs (e.g., nC_{23}) (12, 13). The ratio of shorter- versus long-chain *n*-alkane abundances distinguish relative organic matter inputs from aquatic versus terrestrial plants to sediments (13):

$$P_{aq} = (nC_{23} + nC_{25}) / (nC_{23} + nC_{25} + nC_{29} + nC_{31}).$$

Sedges and ferns are prolific in many tropical ecosystems (14). These plants both have variable and therefore nondiagnostic *n*-alkane profiles. However, sedges produce distinctive phenolic compounds [e.g., 5-*n*-tricosylresorcinol ($^nR_{23}$)] and ferns produce distinctive midchain diols [e.g., 1,13-dotriacontanediol (C_{32}-diol)] (*SI Discussion*).

Lignin monomers provide evidence for woody and nonwoody plants. This refractory biopolymer occurs in both leaves and wood, serves as a structural tissue, and accounts for up to half of the total organic carbon in modern vegetation (11). Lignin is composed of three phenolic monomer types that show distinctive distributions in woody and herbaceous plant tissues. Woody tissues from dicotyledonous trees and shrubs contain syringyl (*S*) and vanillyl (*V*) phenols (12), whereas cinnamyl (*C*) phenols are exclusively found in herbaceous tissues (12). The relative abundance of *C* versus *V* phenols (*C*/*V*) is widely used to distinguish between woody and herbaceous inputs to sedimentary and soil organic matter (15).

Plant biomarker $^{13}C/^{12}C$ ratios (expressed as $\delta^{13}C$ values) are sensitive indicators of community composition, ecosystem structure, and climate conditions (8). Most woody plants and forbs in eastern Africa use C_3 photosynthesis (6), whereas arid-adapted grasses use C_4 photosynthesis (8, 14). These two pathways discriminate differently against ^{13}C during photosynthesis, resulting in characteristic $\delta^{13}C$ values for leaf waxes derived from C_3 (about –36.0‰) and C_4 (–21.0‰) plants (16). Carbon isotopic abundances of phenolic monomers of lignin amplify the C_3–C_4 difference and range between *ca.* –34.0‰ (C_3) and –14.0‰ (C_4) in tropical ecosystems (15). Terrestrial C_3 plant $\delta^{13}C$ values decrease with increased exposure to water, respired CO_2, and shade (8), with lowest values observed in moist regions with dense canopy (17). Although concentration and $\delta^{13}C$ values of atmospheric CO_2

Significance

Humans evolved in response to the availability of plant and water resources over space and through time. Their influence on our species' evolution is debated, though, because archives of their spatial distribution are scarce at early human (hominin) localities. Meter-scale vegetation patterns are revealed from sedimentary plant biomarkers across an archaeological horizon at Olduvai Gorge (FLK *Zinj*). Biomarkers evince a varied local landscape with a woodland patch near a small freshwater wetland, surrounded by an open grassland landscape. Biomarkers from the wetland indicate diverse edible plants near potable water. The coexistence of butchered large animal bones and hominin remains, including juveniles, within an isolated biomarker-delineated wooded microhabitat at FLK *Zinj* provide support for early provisioning behaviors by our ancestors.

Author contributions: C.R.M., G.M.A., M.D.-R., and K.H.F. designed research; C.R.M. performed research; C.R.M. and K.H.F. analyzed data; and C.R.M., G.M.A., M.D.-R., and K.H.F. wrote the paper.

The authors declare no conflict of interest.

This article is a PNAS Direct Submission.

[1]To whom correspondence should be addressed. Email: clayton.magill@erdw.ethz.ch.

This article contains supporting information online at www.pnas.org/lookup/suppl/doi:10.1073/pnas.1507055113/-/DCSupplemental.

can affect C_3 plant $\delta^{13}C$ values (17), this influence is not relevant to our work here, which focuses on a single time window (*SI Discussion*). The large differences in leaf-wax $\delta^{13}C$ values between closed C_3 forest to open C_4 grassland are consistent with soil organic carbon isotope gradients across canopy-shaded ground surfaces (6) and serve as a quantitative proxy for woody cover (f_{woody}) in savannas (8).

As is observed for nonhuman primates, hominin dietary choices were likely shaped by ecosystem characteristics over habitat scales of 1–1,000 m^2 (3–5). To evaluate plant distributions at this small spatial scale (9), we excavated 71 paleosol samples from close-correlated trenches across a ~25,000-m^2 area that included FLK *Zinjanthropus* Level 22 (FLK *Zinj*) at Olduvai Gorge (Fig. 1). Recent excavations (18–21) at multiple trenches at four sites (FLK^{NN}, FLK^{N}, FLK, and FLK^{S}, Fig. 1*D*) exposed a traceable thin (5–50 cm), waxy green to olive-brown clay horizon developed by pedogenic alterations of playa lake margin alluvium (22). Weak stratification and irregular redox stains suggest initial soil development occurred during playa lake regression (18, 22), around 1.848 Ma (ref. 23 and *SI Discussion*). To date, craniodental remains from at least three hominin individuals (18–20), including pre-adolescent early *Homo* and *Paranthropus boisei*, were recovered from FLK *Zinj*. Fossils and artifacts embedded in the paleosol horizon often protrude into an overlying airfall tuff (18, 19), which suggests fossil remains were catastrophically buried in situ under volcanic ash. Rapid burial likely fostered the exceptional preservation of both macrofossils (10) and plant biomarkers across the FLK *Zinj* land surface.

Plant biomarker signatures reveal distinct types of vegetation juxtaposed across the FLK *Zinj* land surface (Figs. 2–4 and Fig. S1). In the northwest, FLK^{NN} trenches show high nC_{23} $\delta^{13}C$ values (Fig. 2*B*) as well as high *C*/*V* and P_{aq} values (Figs. 3 and 4*A*). They indicate floating or submerged aquatic plants (macrophytes) in standing freshwater (13), a finding that is consistent with nearby low-temperature freshwater carbonates (tufa), interpreted to be deposited from spring waters (22). Adjacent FLK^{N} trenches have lower P_{aq} values (Fig. 4*A*) with occurrences of fern-derived C_{32}-diol and sedge-derived $^{n}R_{23}$ (Fig. 2 *C* and *D*). These biomarker distributions indicate an abrupt (around 10 m) transition from aquatic to wetland vegetation. Less than 100 m away (Fig. 1*C*), low nC_{31} $\delta^{13}C$ values (Fig. 2*A*) and low *C*/*V* and very low P_{aq} values (Figs. 3 and 4*A*) collectively indicate dense woody cover (Fig. 4*B*). In the farthest southeastern (FLK^{S}) trenches, high *C*/*V* values and high $\delta^{13}C$ values for *C* lignin phenols (Fig. 3) indicate open C_4 grassland.

Biomarkers define a heterogeneous landscape at Olduvai and suggest an influence of local resources on hominin diets and behavior. It is recognized (2, 24–26) that early *Homo* species and *P. boisei* had similar physiological characteristics. These similarities in physical attributes suggest behavioral differences were what allowed for overlapping ranges and local coexistence

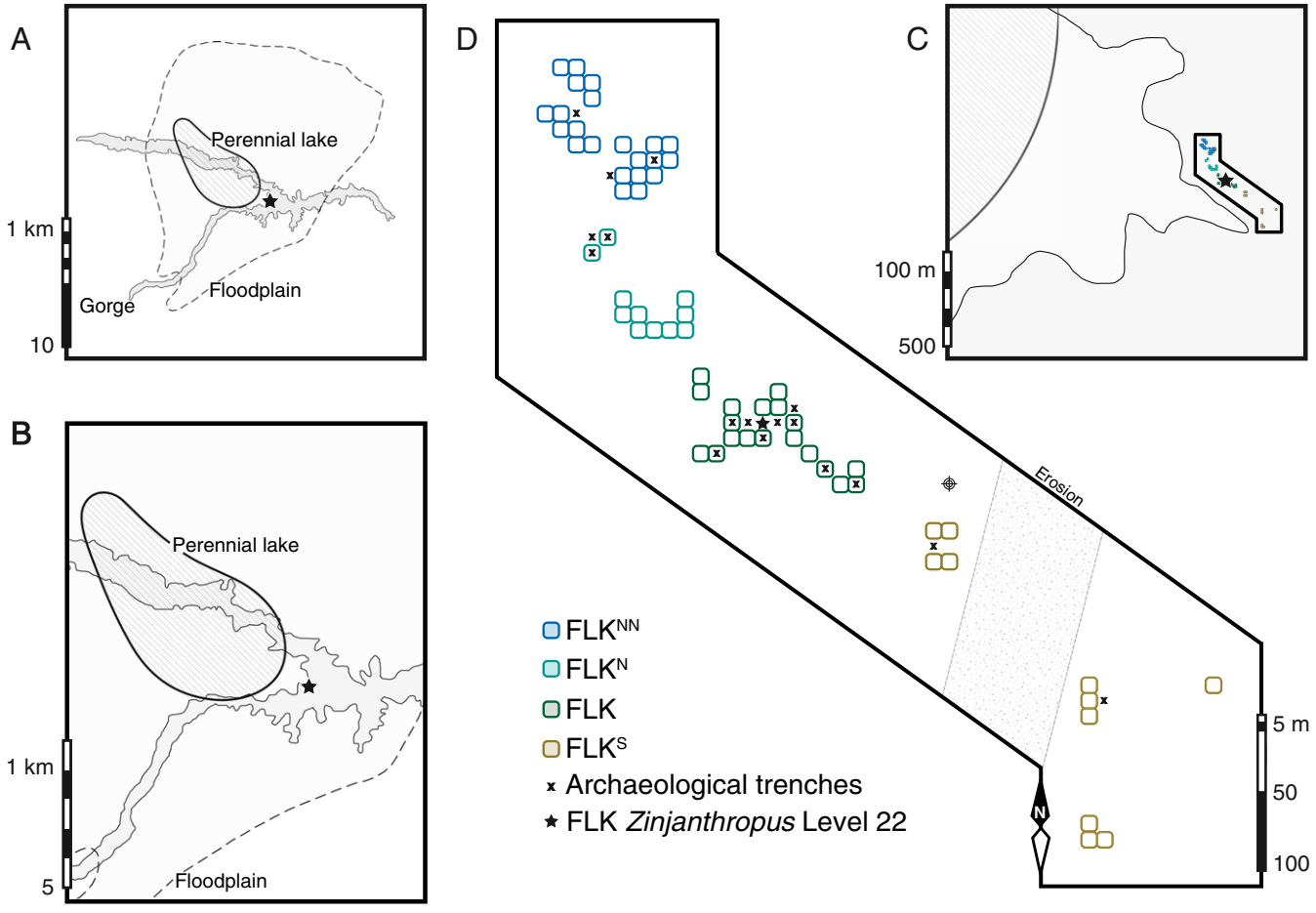

Fig. 1. Location and map of FLK *Zinj* paleosol excavations. (*A* and *B*) Location of FLK *Zinj* as referenced to reconstructed depositional environments at Olduvai Gorge during the early Pleistocene (18, 22) and the modern gorge walls. The perennial lake contained shallow saline–alkaline waters that frequently flooded the surrounding playa margin (i.e., floodplain) flats. (*C*) Outline of FLK *Zinj* paleosol excavation sites used for our spatial biomarker reconstructions. (*D*) Concentric (5 m) gridded distribution map of FLK *Zinj* paleosol excavations relative to previous archaeological trenches (18–21). Major aggregate complexes (FLK^{NN}, FLK^{N}, FLK, and FLK^{S}) are color-coded to show excavation-site associations.

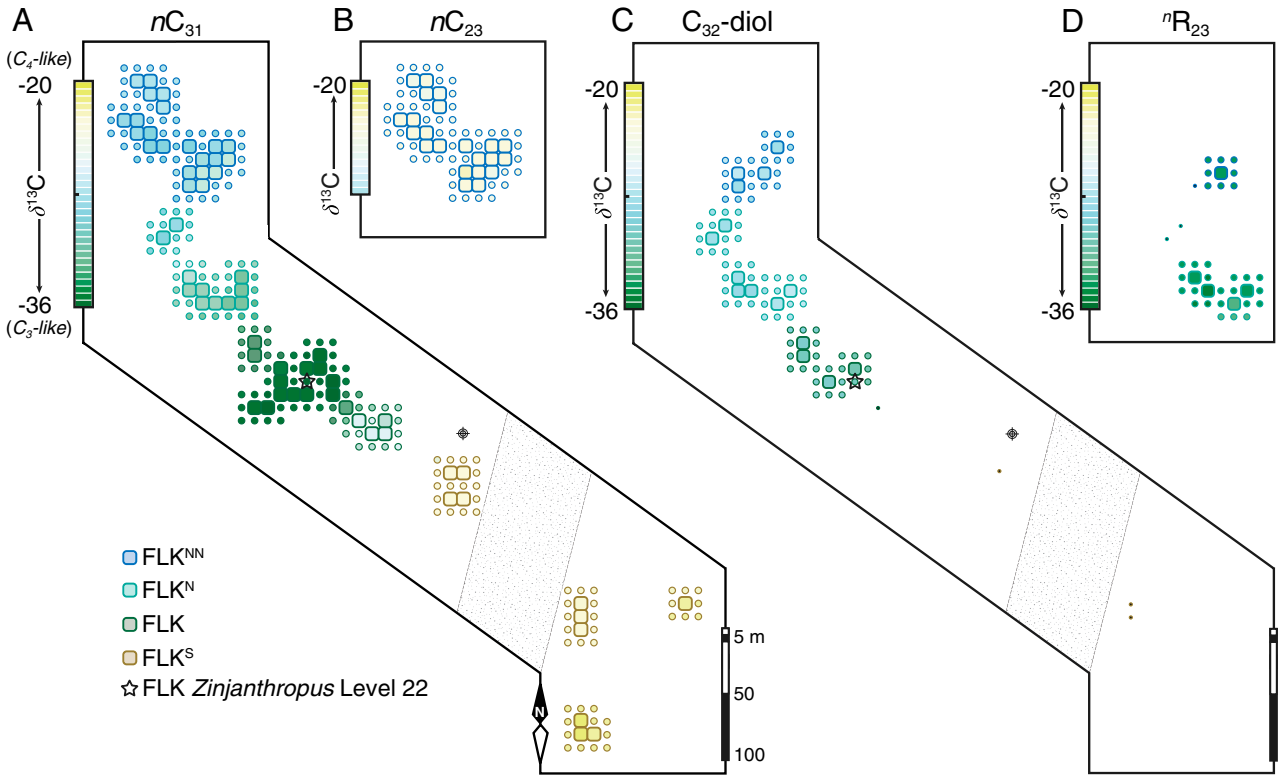

Fig. 2. Spatial distributions and $\delta^{13}C$ values for plant biomarkers across FLK *Zinj*. Measured and modeled $\delta^{13}C$ values (large and smaller circles, respectively) are shown for (*A*) nC_{31} from terrestrial plants, (*B*) nC_{23} from (semi)aquatic plants, (*C*) C_{32}-diol from ferns, and (*D*) $^nR_{23}$ from sedges (see refs. 12 and 13 and *SI Discussion*). Modeled values [inverse distance-weighted (9)] account for spatial autocorrelation (15-m radius) in standing biomass (35) over scales of soil organic matter accumulation (11). Black dots represent paleosols with insufficient plant biomarker concentrations for isotopic analysis.

(sympatry) of both hominins. For instance, differences in seasonal subsistence strategies or different behavior during periods of drought and limited food could have reduced local hominin competition and fostered diversification via niche specialization (27–29).

Physical and isotopic properties of fossil teeth indicate *P. boisei* was more water-dependent [low enamel $\delta^{18}O$ values (24)] and consumed larger quantities of abrasive, ^{13}C-enriched foodstuffs [flat-worn surfaces (25) and high enamel $\delta^{13}C$ values (26)] than coexisting early *Homo* species. Although ^{13}C-enriched enamel is commonly attributed to consumption of C_4 grasses or meat from grazers (14), this was not likely, because *P. boisei* craniodental features are inconsistent with contemporary gramnivores (24, 25) or extensive uncooked flesh mastication (26). Numerous scholars have proposed the nutritious underground storage organs (USOs) of C_4 sedges were a staple of hominin diets (14, 24, 26, 27). Consistent with this suggestion, occurrences of $^nR_{23}$ attest to the presence of sedges at FLK^{NN} and FLK^{N} (Fig. 2*D*). However, the low $\delta^{13}C$ values measured for $^nR_{23}$ at these same sites (Fig. 2*D* and Fig. S2) indicate C_3 photosynthesis (12, 16), a trait common in modern sedges that grow in alkaline wetlands and lakes (30) (Fig. S3). Thus, biomarker signatures support the presence of C_3 sedges in the wetland area of FLK *Zinj*.

Alternative foodstuffs with abrasive, ^{13}C-enriched biomass include seedless vascular plants (cryptogams), such as ferns and lycophytes [e.g., quillworts (27, 30)]. Ferns are widely distributed throughout eastern Africa in moist and shaded microhabitats (31) and are often found near dependable sources of drinking water (32). Today, ferns serve as a dietary resource for humans and nonhuman primates alike (27), and fiddlehead consumption is consistent with the inferred digestive physiology [salivary proteins (33)] and the microwear on molars (34) of *P. boisei* in eastern Africa (25, 26). Ferns were present at FLK^{N}, based on measurements of C_{32}-diol (Fig. 2*D*). Further, the high

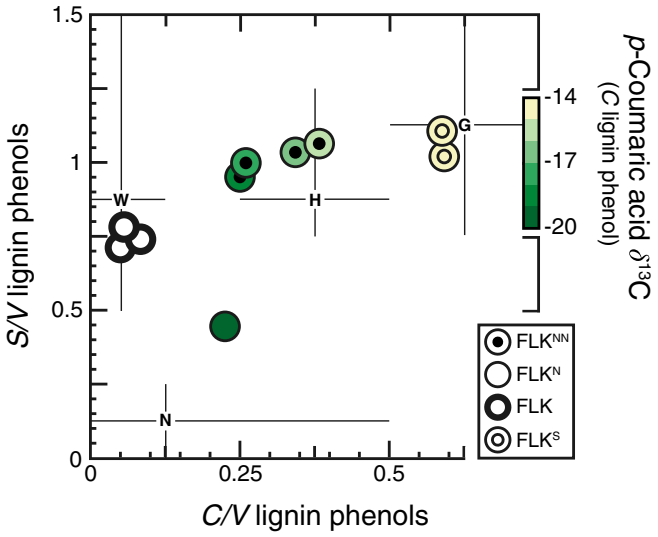

Fig. 3. Molecular and isotopic signatures for lignin phenols across FLK *Zinj*. Bivariate plots are shown for diagnostic lignin compositional parameters (see refs. 12 and 15 and Table S1) associated with aggregate excavation complexes (Fig. 1*C*). Symbols are colored according to respective $\delta^{13}C$ values for the *C* lignin phenol, *p*-coumaric acid. FLK symbols are uncolored due to insufficient *p*-coumaric acid concentrations for isotopic analysis. Representative lignin compositional parameters (12, 15) are shown for monocotyledonous herbaceous tissues (G), dicotyledonous herbaceous tissues (H), cryptogams (N), and dicotyledonous woody tissues (W).

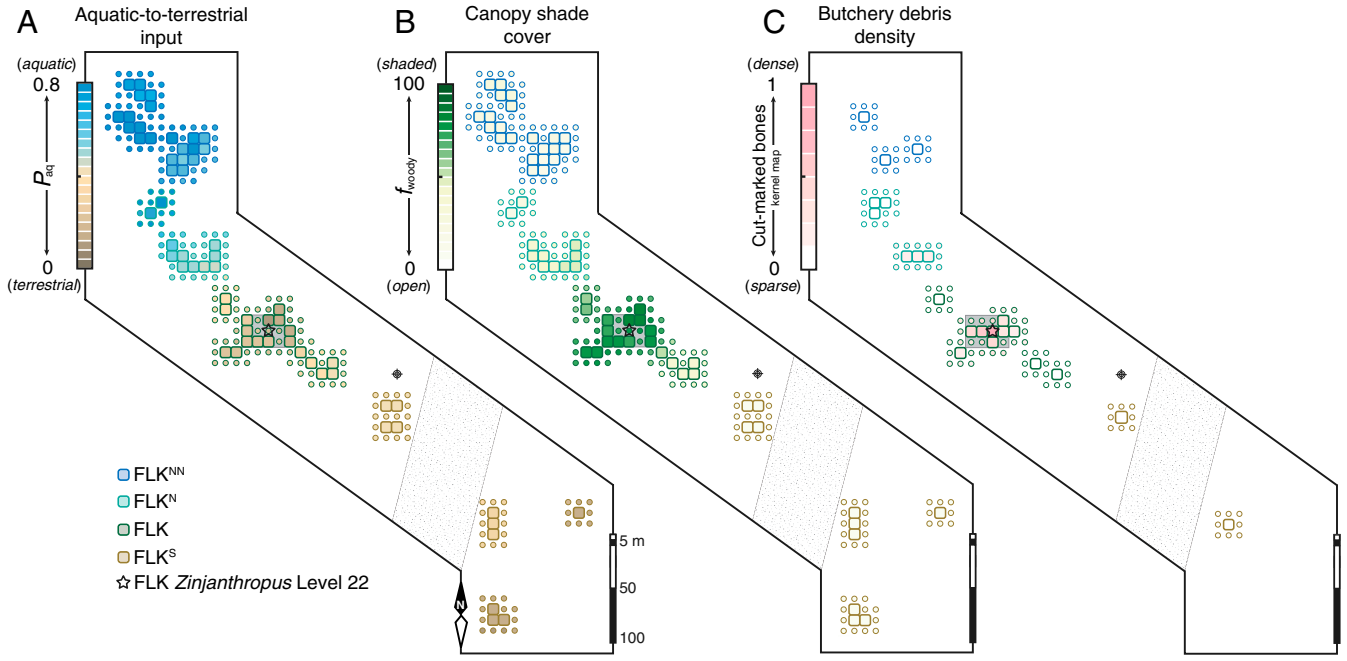

Fig. 4. Spatial relationships shared between local plant resources and hominin remains. Measured and modeled values (large and smaller circles, respectively) are shown for (*A*) P_{aq} (13) and (*B*) f_{woody} (8). Modeled values [inverse distance-weighted (9)] account for spatial autocorrelation (15-m radius) in standing biomass (35) over scales of soil organic matter accumulation (11). (*C*) Kernel density map of cut-marked bones (18–21) across the FLK *Zinj* land surface (Fig. S4). High estimator values indicate hotspots of hominin butchery (Fig. S5). A shaded rectangle captures the area (*ca*. 0.68 probability mass) with highest cut-marked bone densities and is shown in *A* and *B* for reference.

$\delta^{13}C$ values measured for these compounds are consistent with significant fern consumption by *P. boisei* at Olduvai Gorge.

Ferns and grasses were not the only plant foods present during the time window documented by FLK *Zinj*. Further, the exclusive reliance on a couple of dietary resources was improbable for *P. boisei,* because its fossils occur in diverse localities (24–26). Aquatic plants are an additional candidate substrate, as evidenced by high P_{aq} values at FLK^{NN} and FLK^{N} (Fig. 4*A*). Floating and submerged plants proliferate in wetlands throughout eastern Africa today (13, 14), and many produce nutritious leaves and rootstock all year long (27, 28). Although C_4 photosynthesis is rare among modern macrophytes (30), they can assimilate bicarbonate under alkaline conditions, which results in C_4-like isotope signatures in their biomass (30). Their leaf waxes, such as nC_{23} (13), are both present and carry ^{13}C-enriched signatures at FLK^{NN} and FLK^{N} (Fig. 2*B*). It is also likely that aquatic macrophytes sustained invertebrates and fish with comparably ^{13}C-enriched biomass, as they do in modern systems (14), and we suggest aquatic animal foods could have been important in *P. boisei* diets (27, 28).

Biomarkers across the FLK *Zinj* soil horizon resolve clear patterns in the distribution of plants and water and suggest critical resources that shaped hominin existence at Olduvai Gorge. The behavioral implications of local conditions require understanding of regional climate and biogeography (3–5, 7), because hominin species likely had home ranges much larger than the extent of excavated sites at FLK *Zinj*. Lake sediments at Olduvai Gorge include numerous stacked tuffs with precise radiometric age constraints (23). These tephrostratigraphic correlations (21) tie the FLK *Zinj* landscape horizon to published records of plant biomarkers in lake sediments that record climate cycles and catchment-scale variations in ecology. Correlative lake sediment data indicate the wet and wooded microhabitats of FLK *Zinj* sat within a catchment dominated by arid C_4 grassland (8). Under similarly arid conditions today, only a small fraction of landscape area (*ca*. 0.05) occurs within 5 km of either forest or standing freshwater (35). Given a paucity of shaded refuge and potable water in the catchment, the concentration of hominin butchery debris (18–21) exclusively within the forest microhabitat and adjacent to a freshwater wetland (Fig. 4) is notable. We suggest the spatial patterns defined by both macro- and molecular fossils reflect hominins engaged in social transport of resources (1–5), such as bringing animal carcasses and freshwater-sourced foods from surrounding grassy or wetland habitats to a wooded patch that provided both physical protection and access to water.

Materials and Methods

Plant Biomarker Extraction and Isolation. Freeze-dried and powdered paleosol samples (10–20 g dry weight, $n = 71$) were extracted by accelerated solvent extraction (Dionex ASE 200 system) with 90:10 dichloromethane (DCM) to methanol by volume. Total lipid extracts were separated into fractions over activated silica gel by elution with hexane (apolar), DCM, and methanol. Apolar fractions were further separated over silver-impregnated alumina by elution with hexane (saturated apolar). Then, *n*-alkanes were separated from saturated apolar fractions by zeolitic (5 Å) sieve. Once extracted, residual paleosols were oxidized under alkaline conditions and acidified with hydrochloric acid. Lignin phenols were recovered by liquid extraction with diethyl ether. Additional details are provided in *SI Materials and Methods*.

Molecular and Isotopic Analysis. Molecular signatures were characterized by GC-MS (*SI Materials and Methods*). Polar fractions and lignin phenols were derivatized with N,O-bis(trimethylsilyl)trifluoracetamide (BSTFA) in pyridine. Isotopic signatures were characterized by gas chromatography-combustion-isotope-ratio monitoring mass spectrometry and expressed in standard permil (‰) notation relative to Vienna Pee Dee Belemnite (VPDB):

$$\delta^{13}C = 1{,}000\left(R_{sample}/R_{standard} - 1\right),\ R = {}^{13}C/{}^{12}C.$$

ACKNOWLEDGMENTS. We are thankful to Richard Hay (1926–2006), whose pioneering work at Olduvai Gorge inspired this research. We thank the Tanzania Antiquities Department and the Ngorongoro Conservation Area Authority for field permits and support. This research study was supported by the Spanish Ministry of Economy and Competitiveness (HAR2013-45246-C3-1-P) and National Science Foundation Grant DGE 0947962.

1. Marlowe F (2005) Hunter-gatherers and human evolution. *Evol Anthropol* 14(2): 54–67.
2. Winterhalder B (1980) Environmental analysis in human evolution and adaptation research. *Hum Ecol* 8(2):135–170.
3. Potts R (2012) Environmental and behavioral evidence pertaining to the evolution of early *Homo*. *Curr Anthropol* 53(S6):299–317.
4. Kroll E (1994) Behavioral implications of Plio-Pleistocene archaeological site structure. *J Hum Evol* 27(1):107–138.
5. Rose L, Marshall F (1996) Meat eating, hominid sociality, and home bases revisited. *Curr Anthropol* 37(2):307–338.
6. Cerling TE, et al. (2011) Woody cover and hominin environments in the past 6 million years. *Nature* 476(7358):51–56.
7. Kingston JD (2007) Shifting adaptive landscapes: Progress and challenges in reconstructing early hominid environments. *Am J Phys Anthropol* 134(Suppl 45):20–58.
8. Magill CR, Ashley GM, Freeman KH (2013) Water, plants, and early human habitats in eastern Africa. *Proc Natl Acad Sci USA* 110(4):1175–1180.
9. West J, et al. (2010) *Isoscapes: Understanding Movement, Pattern, and Process on Earth Through Isotope Mapping* (Springer, New York).
10. Behrensmeyer A, Kidwell S, Gastaldo R (2000) Taphonomy and paleobiology. *Paleobiology* 26(Sp4):103–147.
11. Kögel-Knabner I (2002) The macromolecular organic composition of plant and microbial residues as inputs to soil organic matter. *Soil Biol Biochem* 34(2):139–162.
12. Amelung W, et al. (2008) Combining biomarker with stable isotope analyses for assessing the transformation and turnover of soil organic matter. *Adv Agron* 100:155–250.
13. Ficken K, et al. (2000) An *n*-alkane proxy for the sedimentary input of submerged/floating freshwater aquatic macrophytes. *Org Geochem* 31(7):745–749.
14. Peters CR, Vogel JC (2005) Africa's wild C_4 plant foods and possible early hominid diets. *J Hum Evol* 48(3):219–236.
15. Huang Y, et al. (1999) $\delta^{13}C$ of individual lignin phenols in Quaternary lake sediments: A novel proxy for deciphering past terrestrial vegetation changes. *Geology* 27(5): 471–474.
16. Hobbie E, Werner R (2004) Intramolecular, compound-specific, and bulk carbon isotope patterns in C_3 and C_4 plants: A review and synthesis. *New Phytol* 161(2):371–385.
17. Diefendorf A, et al. (2015) Paleogene plants fractionated carbon isotopes similar to modern plants. *Earth Planet Sci Lett* 429:33–44.
18. Hay R (1976) *Geology of the Olduvai Gorge* (Univ of California Press, Berkeley, CA).
19. Domínguez-Rodrigo M, et al. (2010) New excavations at the FLK *Zinjanthropus* site and its surrounding landscape and their behavioral implications. *Quat Res* 74(3): 315–332.
20. Blumenschine RJ, et al. (2012) Environments and hominin activities across the FLK Peninsula during *Zinjanthropus* times (1.84 Ma), Olduvai Gorge, Tanzania. *J Hum Evol* 63(2):364–383.
21. Uribelarrea D, et al. (2014) Geo-archaeological and geometrically corrected reconstruction of the 1.84 Ma FLK *Zinj* paleolandscape at Olduvai Gorge, Tanzania. *Quat Int* 322:7–31.
22. Ashley G, et al. (2014) Freshwater limestone in an arid basin: A Goldilocks effect. *J Sed Geol* 84(11):988–1004.
23. Deino AL (2012) $(^{40})Ar/(^{39})Ar$ dating of Bed I, Olduvai Gorge, Tanzania, and the chronology of early Pleistocene climate change. *J Hum Evol* 63(2):251–273.
24. Cerling TE, et al. (2011) Diet of *Paranthropus boisei* in the early Pleistocene of eastern Africa. *Proc Natl Acad Sci USA* 108(23):9337–9341.
25. Smith AL, et al. (2015) The feeding biomechanics and dietary ecology of *Paranthropus boisei*. *Anat Rec (Hoboken)* 298(1):145–167.
26. Macho GA (2014) Baboon feeding ecology informs the dietary niche of *Paranthropus boisei*. *PLoS One* 9(1):e84942.
27. Wrangham R, Cheney D, Seyfarth R, Sarmiento E (2009) Shallow-water habitats as sources of fallback foods for hominins. *Am J Phys Anthropol* 140(4):630–642.
28. Laden G, Wrangham R (2005) The rise of the hominids as an adaptive shift in fallback foods: Plant underground storage organs (USOs) and australopith origins. *J Hum Evol* 49(4):482–498.
29. Stanford CB (2006) The behavioral ecology of sympatric African apes: Implications for understanding fossil hominoid ecology. *Primates* 47(1):91–101.
30. Keeley J, Sandquist D (1992) Carbon: Freshwater plants. *Plant Cell Environ* 15(9): 1021–1035.
31. Aldasoro J, Cabezas F, Aedo C (2004) Diversity and distribution of ferns in sub-Saharan Africa, Madagascar and some islands of the South Atlantic. *J Biogeogr* 31(10): 1579–1604.
32. Jarman P (1972) The use of drinking sites, wallows and salt licks by herbivores in the flooded Middle Zambezi Valley. *Afr J Ecol* 10(3):193–209.
33. Bennick A (2002) Interaction of plant polyphenols with salivary proteins. *Crit Rev Oral Biol Med* 13(2):184–196.
34. Kieser J, et al. (2001) Patterns of dental wear in the early Maori dentition. *Int J Osteoarchaeol* 11(3):206–217.
35. Scholes R, et al. (2002) Trends in savanna structure and composition along an aridity gradient in the Kalahari. *J Veg Sci* 13(3):419–428.
36. Goñi M, Hedges J (1992) Lignin dimers: Structures distribution, and potential geochemical applications. *Geochim Cosmochim Acta* 56(11):4025–4043.
37. Magill C, Denis E, Freeman K (2015) Rapid sequential separation of sedimentary lipid biomarkers via selective accelerated solvent extraction. *Org Geochem* 88:29–34.
38. Avsejs L, et al. (2002) 5-*n*-alkylresorcinols as biomarkers of sedges in an ombrotrophic peat section. *Org Geochem* 33(7):861–867.
39. Speelman E, et al. (2009) Biomarker lipids of the freshwater fern *Azolla* and its fossil counterpart from the Eocene Arctic Ocean. *Org Geochem* 40(5):628–637.
40. Villanueva L, et al. (2014) Potential biological sources of long chain alkyl diols in lacustrine environments. *Org Geochem* 68:27–30.
41. Silverman B (1986) *Density Estimation for Statistics and Data Analysis* (CRC, Boca Raton, FL).
42. Philip G, Watson D (1986) Geostatistics and spatial data analysis. *Math Geol* 18: 505–509.
43. Borgogno F, et al. (2009) Mathematical models of vegetation pattern formation in ecohydrology. *Rev Geophys* 47(1):RG1005.
44. Caylor K, Shugart H (2006) *Pattern and Process in Savanna Ecosystems* (Springer, New York).
45. Wang L, et al. (2009) Spatial heterogeneity and sources of soil carbon in southern African savannas. *Geoderma* 149(3):402–408.
46. Lin YP, Chu HJ, Wu CF, Chang TK, Chen CY (2011) Hotspot analysis of spatial environmental pollutants using kernel density estimation and geostatistical techniques. *Int J Environ Res Public Health* 8(1):75–88.
47. Kozubek A, Tyman JH (1999) Resorcinolic lipids, the natural non-isoprenoid phenolic amphiphiles and their biological activity. *Chem Rev* 99(1):1–26.
48. Tieszen L, et al. (1979) The distribution of C_3 and C_4 grasses and carbon isotope discrimination along an altitudinal and moisture gradient in Kenya. *Oecologia* 37(3): 337–350.
49. Stock W, Chuba D, Verboom G (2004) Distribution of South African C_3 and C_4 species of *Cyperaceae* in relation to climate and phylogeny. *Austral Ecol* 29(3):313–319.
50. Besnard G, et al. (2009) Phylogenomics of C_4 photosynthesis in sedges (Cyperaceae): Multiple appearances and genetic convergence. *Mol Biol Evol* 26(8):1909–1919.
51. Muasya A, et al. (2009) Phylogeny of Cyperaceae based on DNA sequence data: Current progress and future prospects. *Bot Rev* 75(1):2–21.
52. Muasya A, et al. (2011) The Cyperaceae in Madagascar show increased species richness in upland forest and wetland habitats. *Plant Ecol Evol* 144(3):357–362.
53. Larridon I, et al. (2011) Affinities in C_3 *Cyperus* lineages (Cyperaceae) revealed using molecular phylogenetic data and carbon isotope analysis. *Bot J Linn Soc* 167(1):19–46.
54. Larridon I, et al. (2013) Towards a new classification of the giant paraphyletic genus *Cyperus* (Cyperaceae): Phylogenetic relationships and generic delimitation in C_4 *Cyperus*. *Bot J Linn Soc* 172(1):106–126.
55. Adeniyi T, et al. (2014) Investigating the phytochemicals and antimicrobial properties of three sedge (Cyperaceae) species. *Not Sci Biol* 6(3):276–281.
56. Gamal M, et al. (2015) A review: Compounds isolated from *Cyperus* species (Part I): Phenolics and nitrogenous. *Int J Pharmacogn Phytochem* 7:51–67.
57. Nassar M, et al. (2015) Essential oil and antimicrobial activity of aerial parts of *Cyperus leavigatus* L. (Family: Cyperaceae). *J Essent Oil Bear Pl* 18(2):416–422.
58. Gehrke B (2011) Synopsis of *Carex* (Cyperaceae) from sub-Saharan Africa and Madagascar. *Bot J Linn Soc* 166(1):51–99.
59. Ortiz J, et al. (2010) Palaeoenvironmental reconstruction of Northern Spain during the last 8000 cal yr BP based on the biomarker content of the Roñanzas peat bog (Asturias). *Org Geochem* 41(5):454–466.
60. Cho HS, et al. (2013) Inhibition of *Pseudomonas aeruginosa and Escherichia coli* O157: H7 biofilm formation by plant metabolite ε-viniferin. *J Agric Food Chem* 61(29): 7120–7126.
61. Jetter R, Riederer M (1999) Long-chain alkanediols, ketoaldehydes, ketoalcohols and ketoalkyl esters in the cuticular waxes of *Osmunda regalis* fronds. *Phytochemistry* 52(5):907–915.
62. Christenhusz MJ, Chase MW (2014) Trends and concepts in fern classification. *Ann Bot (Lond)* 113(4):571–594.
63. Sage R (2002) Are crassulacean acid metabolism and C_4 photosynthesis incompatible? *Funct Plant Biol* 29(6):775–785.
64. Kornas J (1985) Adaptive strategies of African pteridophytes to extreme environments. *P Roy Soc Edin B* 86:391–396.
65. Keeley J (1998) CAM photosynthesis in submerged aquatic plants. *Bot Rev* 64(2):121–175.
66. Rascio N (2002) The underwater life of secondarily aquatic plants: some problems and solutions. *Crit Rev Plant Sci* 21(4):401–427.
67. Raven J, et al. (2008) The evolution of inorganic carbon concentrating mechanisms in photosynthesis. *Proc R Soc B Biol Sci* 363(1504):2641–2650.
68. Smith J, Winter K (1996) *Crassulacean Acid Metabolism* (Springer, Berlin).
69. Holtum J, Winter K (1999) Degrees of crassulacean acid metabolism in tropical epiphytic and lithophytic ferns. *Funct Plant Biol* 26(8):749–757.
70. Holtum J, et al. (2005) Carbon isotope composition and water-use efficiency in plants with crassulacean acid metabolism. *Funct Plant Biol* 32(5):381–388.
71. Ehleringer J, et al. (1987) Leaf carbon isotope ratios of plants from a subtropical monsoon forest. *Oecologia* 72(1):109–114.
72. Bunn S, Boon P (1993) What sources of organic carbon drive food webs in billabongs? A study based on stable isotope analysis. *Oecologia* 96(1):85–94.
73. Zotz G (2004) How prevalent is crassulacean acid metabolism among vascular epiphytes? *Oecologia* 138(2):184–192.
74. Anthelme F, et al. (2011) Are ferns in arid environments underestimated? Contribution from the Saharan Mountains. *J Arid Environ* 75(6):516–523.
75. Stanistreet IG (2012) Fine resolution of early hominin time, Beds I and II, Olduvai Gorge, Tanzania. *J Hum Evol* 63(2):300–308.
76. Fernández-Jalvo Y, et al. (1998) Taphonomy and palaeoecology of Olduvai bed-I (Pleistocene, Tanzania). *J Hum Evol* 34(2):137–172.
77. Bunn H (2007) Meat made us human. *Evolution of the Human Diet: The Known, the Unknown, and the Unknowable* (Oxford Univ Press, Oxford), pp 191–211.
78. Sikes NE, Ashley GM (2007) Stable isotopes of pedogenic carbonates as indicators of paleoecology in the Plio-Pleistocene (upper Bed I), western margin of the Olduvai Basin, Tanzania. *J Hum Evol* 53(5):574–594.
79. Bird M, et al. (1996) A latitudinal gradient in carbon turnover times in forest soils. *Nature* 381(6578):143–146.
80. Krull E, et al. (2005) Recent vegetation changes in central Queensland, Australia: Evidence from $\delta^{13}C$ and ^{14}C analyses of soil organic matter. *Geoderma* 126(3):241–259.

81. Krull E, et al. (2006) Compound-specific $\delta^{13}C$ and $\delta^{2}H$ analyses of plant and soil organic matter: A preliminary assessment of the effects of vegetation change on ecosystem hydrology. *Soil Biol Biochem* 38(11):3211–3221.
82. Bamford MK (2012) Fossil sedges, macroplants, and roots from Olduvai Gorge, Tanzania. *J Hum Evol* 63(2):351–363.
83. Brett R (1991) *The Biology of the Naked Mole Rat* (Princeton Univ Press, Princeton).
84. Karrfalt E (1977) Substrate penetration by the corm of *Isoëtes*. *Am Fern J* 67(1):1–4.
85. Hagemann W (1984) *Morphological Aspects of Leaf Development in Ferns and Angiosperms* (Elsevier, Amsterdam).
86. Denny P (1985) *The Ecology and Management of African Wetland Vegetation* (Springer, Berlin).
87. Yeakel J, et al. (2007) The isotopic ecology of African mole rats informs hypotheses on the evolution of human diet. *Proc R Soc B Biol Sci* 274(1619):1723–1730.
88. Schoeninger M, et al. (2001) Composition of tubers used by Hadza foragers of Tanzania. *J Food Compos Anal* 14(1):15–25.
89. van der Merwe N (2013) Isotopic ecology of fossil fauna from Olduvai Gorge at *ca.* 1.8 Ma, compared with modern fauna. *S Afr J Sci* 109(11-12):1–14.
90. Harris J, Cerling T (2002) Dietary adaptations of extant and Neogene African suids. *J Zool (Lond)* 256(1):45–54.
91. Mugangu T, Hunter M (1992) Aquatic foraging by *Hippopotamus* in Zaire: response to a food shortage? *Mammalia* 56(3):345–350.
92. Sillen A (1988) Elemental and isotopic analyses of mammalian fauna from southern Africa and their implications for paleodietary research. *Am J Phys Anthropol* 76(1): 49–60.
93. Nowak R (1999) *Walker's Mammals of the World* (Johns Hopkins Univ Press, Baltimore).
94. Roth H, et al. (2004) Distribution and status of the hippopotamids in the Ivory Coast. *Afr Zool* 39(2):211–224.
95. Simpson E, et al. (2007) Phylogeny of Cyperaceae based on DNA sequence data-a new rbcL analysis. *Aliso* 23(1):72–83.
96. Jung J, Choi HK (2013) Recognition of two major clades and early diverged groups within the subfamily Cyperoideae (Cyperaceae) including Korean sedges. *J Plant Res* 126(3):335–349.
97. Sheather S, Jones M (1991) A reliable data-based bandwidth selection method for kernel density estimation. *J R Stat Soc B* 53:683–690.

Supporting Information

Magill et al. 10.1073/pnas.1507055113

SI Materials and Methods

Plant Biomarker Extraction. Freeze-dried and powdered paleosols (~20–40 g) were extracted by accelerated solvent extraction (Dionex ASE 200 system) with DCM and methanol (90:10 by volume) in three cycles of 5 min at 100 °C and 1,500 psi (10.3 MPa). Then, extracted paleosols were oxidized under alkaline conditions with cupric oxide at 155 °C for 180 min in stainless steel pressure vessels (36) and then acidified with hydrochloric acid. Oxidation products (lignin phenols) were recovered by extraction with diethylether (36).

Lipid Biomarker Isolation. Total lipid extracts were separated into apolar (hydrocarbon), intermediate-polarity, and polar fractions over activated silica gel by elution with hexane, DCM, and methanol, respectively. Hydrocarbons were separated further into saturated and unsaturated fractions over activated silver-impregnated (5% by weight) silica gel by elution with hexane and DCM, respectively (37). In turn, saturated hydrocarbons were separated further into unbranched (*n*-alkanes) and branched fractions via a zeolitic (5 Å) sieve.

Molecular Characterization. Plant biomarkers were characterized by GC-MS with a Hewlett-Packard 6890 series GC and Hewlett-Packard 5973 mass selective detector. Samples were injected in splitless mode onto a 60-m DB5 fused-silica column (0.32 mm × 0.25 μm) via a Hewlett-Packard 7683 series autosampler. GC temperature was programmed to 60 °C for 1 min then ramped to 320 °C at 6 °C·min^{-1} and held at final temperature for 20 min. Injector and detector temperatures were held at 320 °C. Functionalized biomarkers were derivatized with BSTFA and detected as trimethylsilyl (TMS) derivatives, and 5-*n*-alkylresorcinols were identified based on characteristic mass spectral fragment ions at *m*/*z* 268 (base peak) and *m*/*z* 281 (38). Midchain (1,ω20) diols were identified based on *m*/*z* 369 (base peak) and *m*/*z* 359 (39, 40).

Isotopic Characterization. Isotopic signatures were characterized by gas chromatography-combustion-isotope-ratio monitoring mass spectrometry with a Varian 3400 model GC connected to a Thermo MAT 252. Samples were injected in splitless mode onto a 60-m DB5 fused-silica column (0.32 mm × 0.25 μm) before combustion over nickel and platinum wire with oxygen in helium at 1,000 °C. Values were determined relative to reference gas calibrated to VPDB and expressed in permil (‰) units:

$$\delta^{13}\mathrm{C} = 1{,}000\left(R_{\mathrm{sample}}/R_{\mathrm{standard}} - 1\right), R = {}^{13}\mathrm{C}/{}^{12}\mathrm{C}.$$

Within-run precision (1σ) and accuracy were determined by co-injected internal standards and are equal, respectively, to 0.14‰ and 0.09‰ (*n*-alkanes, $n = 136$), to 0.49‰ and 0.17‰ (diols; $n = 48$), and to 0.66‰ and 0.21‰ (lignin phenols; $n = 40$). Lignin phenol δ^{13}C values are reported for vanillic, syringic, and *p*-coumaric acids (Table S1). Alcoholic and acidic functional groups of lignin phenols were derivatized using BSTFA. Isotopic corrections for carbons added by BSTFA were made via measurements of the δ^{13}C of benzene-1,2-dicarboxylic acid [commonly called phthalic acid (Schimmelmann standards)] after derivatization and then correcting for the mass-balanced δ^{13}C value of derivative carbon (15).

Spatial Analysis. Paleosol excavations were referenced to concentric (5 m) quadrats after geometric correction (0.42°) for tectonic deformation and sediment compaction (21). This approach accounts for uneven spatial distributions in point density (41), enabling accurate distance representations in 2D interpolations (9).

Because plant biomarker reconstructions represent the sum of complex biogeochemical processes across space (9), we use a data-based (deterministic) spatial model based on inverse distance-weighted interpolations of all points within a fixed radius (see ref. 42). Based on combined theory (43) and modern observation (43–45), we calibrate our model with a 15-m radius to account for spatial autocorrelation in standing biomass over scales of soil organic matter accumulation (11). We converted spatially explicit point interpolations into probability surfaces assuming a unimodal (Gaussian) distribution (9, 41, 42). Derivative kernel density maps accurately represent primary spatial patterns (46) and facilitate comparison between diverse datasets with dissimilar resolution.

SI Discussion

Sedge Alkylresorcinols. Resorcinolic compounds have been isolated from plants, algae, and bacteria (47). Odd-numbered long-chained 5-*n*-alkylresorcinol homologs are characteristic of the monocotyledonous plant (sub)families *Pooideae* and *Cyperaceae*. In eastern Africa, extant genera of *Pooideae* are limited to high-altitude environments [>2,000 m (48)], well above the mean elevation of Olduvai Gorge (*ca*. 1,450 m). In contrast, extant genera of *Cyperaceae* are quite cosmopolitan, occurring in wetlands and seasonal floodplains from sea level to about 2,000 m (48, 49). Tropical Africa contains around 1,400 *Cyperaceae* species, of which ~50% occur in just two genera: *Cyperus* and *Carex* (50–54). Recent DNA data suggest that C_4 *Cyperus* form a monophyletic clade nested within *Cyperus sensu stricto* (53, 54) and comprise nine segregate genera. Together with earlier descriptive studies about the resorcinolic compounds of C_4 *Cyperus* sedges (e.g., *Cyperus longus*) in northern and East Africa (55, 56), our new analyses of *Cyperus papyrus* (Fig. S2) suggest that 5-*n*-alkylresorcinols with saturated C_{19}–C_{25} side chains occur in *Cyperus* sections of *Rotundi* Clarke and *Papyrus* (54). Earlier studies also indicate alkylresorcinols occur in taxa of the *Cyperus* segregate, *Pycreus* sedges (51, 55, 57) across northeast Africa (58). Importantly, $^{n}R_{23}$ δ^{13}C values for *C. papyrus* are much higher [–21.5 ± 0.5‰ ($n = 3$)] than measured at FLK *Zinj* (Fig. S2).

Cyperus and *Pycreus* (54) are within the cardinal tribe Cypereae, which is one of two major clades of the subfamily Cyperoideae (Fig. S3). The other major clade of this subfamily possesses cardinal tribes called Cariceae and Scirpeae (50, 53), which include widespread African sedges of the genera *Carex* and *Eriophorum* (58), respectively. We found *Carex trisperma* contains significant $^{n}R_{23}$ with low δ^{13}C values [–29.6 ± 1.1‰ ($n = 4$)], and this corroborates earlier data for cosmopolitan species of *Carex* and *Eriophorum* (38, 59, 60). Thus, 5-*n*-alkylresorcinols with saturated C_{19}–C_{25} side chains occur in (sub)tropical tribes of Cyperoideae that include C_4 and C_3 clades (53, 54).

Fern Alkyldiols. Midchain diols derive from a variety of marine, freshwater, and terrestrial photosynthetic organisms (40, 61) and can preserve in sediments and soils over geologic timescales (39). In general, longer midchain diols occur as a series of even-numbered homologs with characteristic isomer distributions (40). Previous studies identify terminal C_{30}–C_{32} diols with ω20 hydroxyl positions (e.g., C_{32}-diol) as diagnostic molecular constituents in ferns (39, 61), and we identified the same major homologs in paleosols around FLK *Zinj* (Fig. S2).

Strict C_4 photosynthesis is not found in monilophytes [ferns (62)] or related lycophytes (63), but these common vascular cryptogams (64) often use alternative carbon-concentrating pathways [e.g., crassulacean acid metabolism (CAM)] that lead to similarly ^{13}C-enriched lipids and biomass (30, 65–70). In subtropical Africa, ferns can show variable degrees of CAM (69–71), and their associated bulk $\delta^{13}C$ values span at least 14‰, from C_3 (~−34‰) to more C_4-like (−20‰) signatures (39, 71–73). Other edible vascular cryptogams with CAM [e.g., *Isoëtes* sp. (14, 65)] likewise are common in seasonal freshwater semiaquatic environments across southern and East Africa (64, 74) and have even more ^{13}C-enriched C_4-like signatures (30, 65, 70, 73).

Sedimentation and Landscape Relief During Paleosol Formation. Recent landscape reconstructions disagree on interpreted sediment facies and stratigraphic correlations around FLK *Zinj* (see refs. 18–21). These differences largely reflect different interpretations of the origin of local topographic relief. Here, we adopt the approach of Uribelarrea et al. (21), which links sediment facies analyses with geomorphic models (Fig. S4) for stratigraphic correlations and landscape reconstruction. An alternative model that FLK *Zinj* was developed by gradational fluvial incision or surface erosion (20) is not supported by this approach. Instead, cumulative evidence suggests low-energy processes dominated during sediment deposition at FLK *Zinj* and that a paleosol surface developed during lake regression from tuffaceous clays and was catastrophically overlain with volcanic ash [Tuff I^C (21)].

The exact timespan represented by paleosols around FLK *Zinj* is debated but constrained by high-precision radiometric ages and taphonomic data. Although Tuff I^C lies about 100 cm above Tuff I^B, they have indistinguishable argon–argon ages of 1.848 ± 0.008 Ma and 1.848 ± 0.003 Ma (23), which set the maximum duration of this entire sequence at 0.011 Ma (75). Taphonomic studies indicate archaeological materials at FLK *Zinj* accumulated during a time window with a duration that was somewhere between several successive seasons up to a century (4, 18–20, 76, 77). These short durations are estimated from an accumulation span of 50–100 y derived from the sedimentation rate (0.1–0.4 $mm \cdot y^{-1}$) during paleosol formation at FLK *Zinj* (75, 78), the *ca*. 50-y residence time of organic carbon in modern (sub)tropic surface soil horizons [0–10 cm (6, 79–81)], and our average sample depth resolution (~0–20 mm underneath Tuff I^C).

Prior Constraints on *P. boisei* Dietary Behavior. Nonspecific plant and animal fossils complement plant biomarker signatures to provide heuristic constraints on the local distributions and availability of food resources around FLK *Zinj*. Scattered leaf impressions bearing parallel longitudinal striations occur at southern FLK^{NN} and FLK^N (19, 20, 82) alongside *Heterocephalus* [African mole-rat (83)] fossils (18, 76) and corroborate plant biomarker signatures in suggesting that C_3 graminoids [e.g., *Typha* (19, 82)] were locally abundant around FLK *Zinj* (Fig. 2 and Fig. S1). Further, silicified culms in sediments underlying FLK *Zinj* (17, 82) resemble the edible USOs (e.g., corms) of African cryptogams [e.g., *Isoëtes* (84, 85)], which often show lower $\delta^{13}C$ values due to C_3–C_4 intermediate photosynthesis (30, 65, 69, 70). Proximate playa lakeshore vegetation was an unlikely source for edible C_4 grasses and sedges, because saline-alkaline water bodies [e.g., paleolake Olduvai (18)] are characteristically devoid of aquatic and emergent C_4 macrophytes (86).

Dietary behavior in *P. boisei* is further informed by enamel $\delta^{13}C$ values for contemporaneous animals in eastern and southern Africa during the early Pleistocene. Enamel $\delta^{13}C$ values of *P. boisei* are markedly high relative to modern and fossil *Heterocephalus* species with specialized USO-rich diets (87), suggesting limited USO consumption by *P. boisei*. Besides, most wild USOs are innutritious without extensive extraoral processing or roasting (88). Rather, *P. boisei* shows enamel $\delta^{13}C$ values intermediate between fossil *Hippopotamus* (hippos) and *Phacochoerus* (pigs) in eastern Africa (24, 89). Based on combined isotopic (89) and craniodental (24) evidence from individual fossils at Olduvai Gorge, both taxa consumed tough browse-graze vegetation (90) such as ferns (91–94), suggesting similar dietary and characteristics for *P. boisei*.

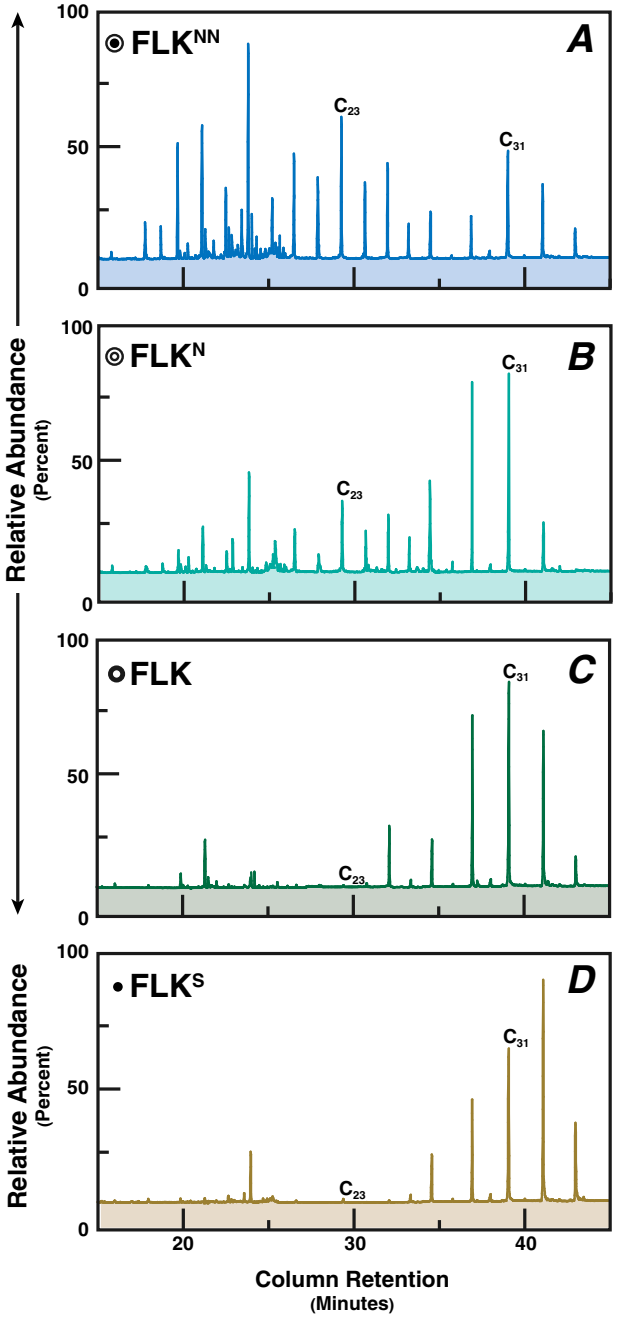

Fig. S1. Total ion chromatograms for saturated hydrocarbons in representative paleosols at (*A*) FLK^{NN}, (*B*) FLK^{N}, (*C*) FLK, and (*D*) FLK^{S}. C_{23}, tricosane; C_{25}, pentacosane; C_{29} nonacosane; C_{31}, hentriacontane.

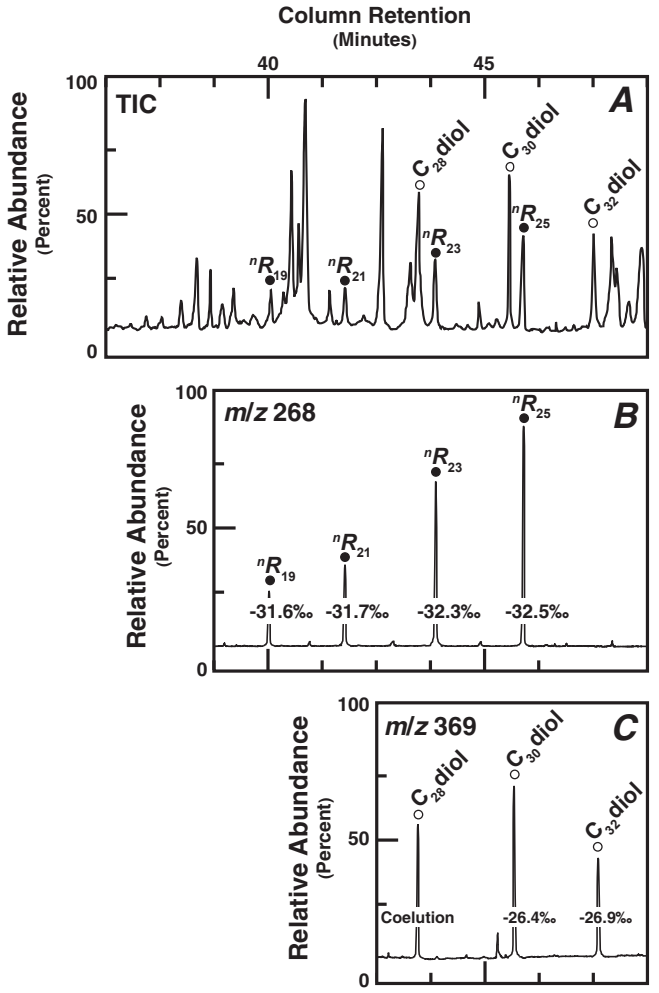

Fig. S2. Total ion chromatogram [TIC (*A*)] and selected ion chromatograms for derivatized 5-*n*-alkylresorcinols [*m/z* 268 (●)] and midchain diols [*m/z* 369 (○)] from a representative paleosol at FLK^{N}. Also shown are $\delta^{13}C$ values for homologous (*B*) 5-*n*-alkylresorcinols and (*C*) midchain diols. C_{32}-diol, dotriacontanediol; $^{n}R_{23}$, tricosylresorcinol.

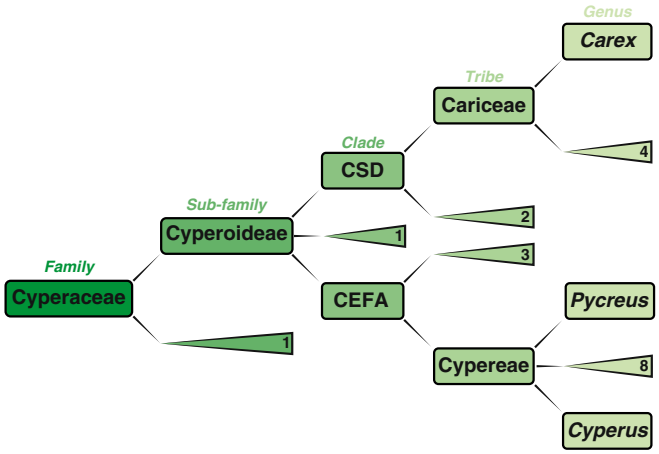

Fig. S3. Summary phyogenetic consensus tree of Cyperaceae (sedges) based on nucleotide (rcbL and ETS1f) sequence data (50–54, 95, 96). Important taxonomic distinctions discussed in *SI Discussion*, *Fern Alkyldiols* are shown explicitly. Triangle-enclosed digits represent the number of additional branches at different levels of taxonomic classification. CEFA, Cypereae Eleocharideae Fuireneae Abildgaardieae; CSD, Cariceae Scirpeae Dulichieae.

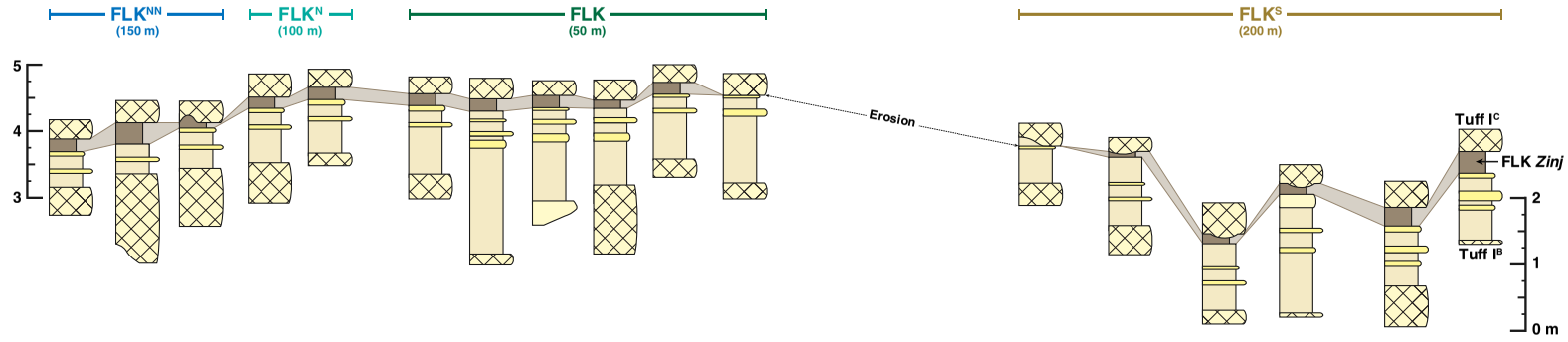

Fig. S4. Schematic representation of the associated Tuff I^B to Tuff I^C stratigraphic sequences at FLK *Zinj* paleosol excavations after geometric correction (0.42°) for tectonic deformation and sediment compaction (21). The FLK *Zinj* soil horizon is shown in brown and traced between excavation sites. Excavation complexes are color-coded to match Figs. 1, 2, and 4). Distances shown under each excavation complex represent their associated (horizontal) transect lengths.

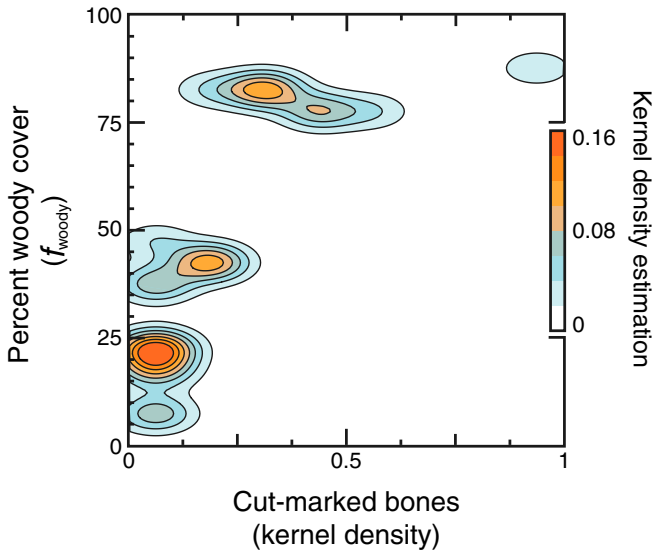

Fig. S5. Bivariate kernel density estimation with paired values ($n = 22$) for woody cover and cut-marked bone density. Contours envelope estimations of 2D (axis-aligned) kernel density. Bandwidths were selected using the direct plug-in approach (97) over binned (5% and 0.125) grid space. Warmer colors are indicative of higher densities.

Table S1. Summary of plant biomarker signatures around FLK *Zinj*

			$\delta^{13}C_{Biomarker}$			
Plant biomarker	Source vegetation	Complex	Average	SD	*n*	[Biomarker], μg·g^{-1} C
nC_{23}	Aquatic plants	FLK^{NN}	−23.4	0.6	27	4
		FLK^{N}	−24.7	1.2	12	3
nC_{31}	Terrestrial plants	FLK^{NN}	−26.6	1.3	27	4
		FLK^{N}	−29.7	1.1	12	4
		FLK	−33.8	0.9	19	7
		FLK^{S}	−21.9	0.6	12	12
$^{n}R_{23}$	Sedges	FLK^{NN}	−33.8	0.3	2	1
		FLK^{N}	−32.0	0.9	5	2
C_{32}-diol	Ferns	FLK^{NN}	−26.7	0.5	5	2
		FLK^{N}	−27.1	0.5	8	6
		FLK	−30.3	0.7	4	2
V	Vascular plants	FLK^{NN}	−24.4*	1.0	4	182
		FLK^{N}	−24.0*	—	1	207
		FLK	−33.6*	0.2	3	111
		FLK^{S}	−17.5*	0.4	2	159
S	Angiosperms	FLK^{NN}	−23.0†	1.2	4	184
		FLK^{N}	−24.9†	—	1	93
		FLK	−33.2†	0.2	3	84
		FLK^{S}	−14.5†	0.2	2	167
C	Herbaceous	FLK^{NN}	−17.9‡	1.3	4	55
		FLK^{N}	−19.4‡	—	1	47
		FLK^{S}	−14.2‡	0.1	2	92

C, [*p*-coumaric acid + ferulic acid]; *S*, [syringaldehyde + acetosyringone + syringic acid]; *V*, [vanillin + acetovanillone + vanillic acid].
*Vanillic acid (TMS derivative).
†Syringic acid (TMS derivative).
‡*p*-coumaric acid (TMS derivative).